Chemotactic agents combining spatial and temporal gradient-sensing boost spatial comparison if they are large, slow, and less persistent

Julian Rode[1], Maja Novak[1,2], Benjamin M. Friedrich[1*]

[1] TU Dresden, Germany.
[2] University of Zagreb, Croatia.

*Corresponding author(s). E-mail(s): benjamin.m.friedrich@tu-dresden.de;

Abstract

Biological cells and small organisms navigate in concentration fields of signaling molecules using two fundamental gradient-sensing strategies: spatial comparison of concentrations measured at different positions on their surface, or temporal comparison of concentrations measured at different locations visited along their motion path. It is believed that size and speed dictate which gradient-sensing strategy cells choose, yet this has never been formally proven. Using information theory, we investigate the optimal gradient-sensing mechanism from the perspective of an ideal chemotactic agent that combines spatial and temporal comparison. We account for physical limits of chemo-sensation: molecule counting noise at physiological concentrations, and motility noise inevitable at the micro-scale. Our simulation data collapses onto an empirical power-law that predicts an optimal weighting of information as function of motility and sensing noise, demonstrating how spatial comparison becomes more beneficial for agents that are large, slow and less persistent. This refines and quantifies the previous heuristic notion. Our idealized model provides a base-line for biological chemotaxis and may inspire the design of robots guided by scalar fields.

Keywords: navigation, chemotaxis, sensing noise, motility noise, stochastic filtering, information decomposition, bearing tracking

Contents

1 Main **2**

1.1 Spatial and temporal comparison 4

1.2 Bayesian chemotaxis combing spatial and temporal comparison 5

1.3 Stereotypic navigation in absence of motility noise 6

1.4 Information flow balance with motility noise 8

1.5 Relative importance of spatial comparison 10

1.6 A phototactic robot 13

2 Discussion **14**

3 Methods **16**

3.1 Analytical theory 16

4 Data availability **20**

5 Code availability **20**

6 Acknowledgments **21**

7 Supplementary information **21**

1 Main

Nature invented two strategies of gradient-sensing for chemotaxis [1–3]: *spatial comparison* (SC), where a biological cell measures the external concentration of signaling molecules simultaneously at different positions on its surface, enabling it to directly estimate a spatial concentration gradient [4–8], and *temporal comparison* (TC), where a cell moves actively and determines whether the local concentration measured sequentially along its path increases or decreases in time [9–13]. Small bacteria such as *E. coli*

employ TC, while larger and slower eukaryotic cells commonly employ SC. Gradient-sensing allows these cells to move up concentration gradients. This chemotaxis enables bacteria to forage for food [9–11], social amoeba to aggregate [5–8], or immune cells to migrate to inflammation sites [4]. Sperm cells of marine invertebrates use a mixed strategy of temporal sampling along chiral paths to find the egg [14]. What is common to these examples is the paramount presence of noise.

In seminal work, Berg and Purcell investigated physical limits of chemosensation in light of sensing and motility noise [15]. Cells sense extracellular concentrations by detecting stochastic binding events of signaling molecules to specialized receptors on their surface, which, even if intracellular signaling were perfect, comprises inevitable molecule counting noise. Thermal noise and active fluctuations during cell migration cause motility noise that randomizes cell orientation, rendering previous estimates of gradient direction uncertain [1, 15]. The Berg-Purcell limit was later refined and fundamental sensing limits for either pure SC or TC derived, see [16, 17] for SC, and [18–21] for TC. It was shown that biological cells operate at the information-theoretic limits of gradient sensing during chemotaxis if concentration gradients are shallow, see [6, 7, 22] for SC, [12, 13, 23, 24] for TC.

Yet, the elementary question, which gradient-sensing strategy is optimal in which noise regime and for which cell size remains unanswered. To address this open question, we build on recent advances in information-theoretically optimal navigation strategies [25–27], which serve as base-line for the chemotaxis of biological cells [13]. Vergassola and co-workers pioneered Bayesian chemotaxis, describing an idealized chemotactic agent that continuously updates a spatial likelihood map of putative target position based on noisy concentration measurements [25]. A focus of this and follow-up studies was tracking odor plumes in turbulent conditions [26, 28, 29] and dynamic gradients [30, 31], which are particularly pronounced at the macroscale. Microscopic agents such as biological cells perceive more regular microscale gradients [32, 33]. Here, we focus

on microscopic agents in static gradients. These agents can be considered as idealized biological cells with unlimited information processing capabilities. A recent mathematical theory developed by Andrea Auconi advanced the *infotaxis* model of Vergassola to spatially extended agents [34]. Here, we build on this theory, which we interpret as agents performing both SC and TC. Additionally, several works investigated optimal filtering and efficient decision strategies for chemotaxis [35–38]. We combine these advances to dissect the optimal weighting of SC and TC in agents capable of both, akin to a nonlinear Kalman filter that optimally weights different noise-corrupted information sources [39]. We quantitatively show how SC becomes increasingly beneficial for agents of larger size that move slowly and with less directional persistence, providing an explanation why crawling eukaryotic cells use SC and most bacteria use TC.

1.1 Spatial and temporal comparison

Principally, chemotactic agents are characterized by their size a, speed v, as well as a sensing rate J_0 at which chemoattractant molecules are detected, which may be assumed linear in concentration c as $J_0 = \lambda c$ [15], with rate constant λ that gauges sensing noise. Motility noise randomizes the direction of motion with effective rotational diffusion coefficient D_{rot}.

An agent of finite size a can detect concentration differences across its diameter, with corresponding signal-to-noise ratio of gradient sensing by SC [7, 16, 36]

$$\mathrm{SNR}^{\mathrm{SC}} = \frac{a^2 t\, \lambda |\nabla c|^2}{c} \quad , \tag{1}$$

where t denotes measurement time.

Alternatively, for gradient-sensing by TC, active motion enables agents to detect concentration changes at a rate $v\,\nabla c$ along their trajectory, with a signal-to-noise ratio

that increases with the cubic power of measurement time t [21]

$$\mathrm{SNR}^{\mathrm{TC}} = \frac{v^2 t^3 \, \lambda |\nabla c|^2}{c} \quad . \tag{2}$$

It has been proposed that effective measurement times are set by the rotational diffusion time $t \sim D_{\mathrm{rot}}^{-1}$ on which swimming direction becomes randomized [1, 40], though recent works suggest more general power-laws [37, 38].

1.2 Bayesian chemotaxis combing spatial and temporal comparison

We present a minimal model of an ideal chemotactic agent combining SC and TC, to dissect the relative importance of SC for finding a target at the center of a radial concentration profile $c(\mathbf{x})$ of signaling molecules. The agent is characterized by size a, a rate constant of molecule detection λ, and rotational diffusion coefficient D_{rot}, see Fig. 1.

The agent continuously updates a likelihood map $p(\mathbf{x})$ of relative target position, based on the timing of molecule detection events *and* the position of detection on its circumference using Bayesian inference, see Eq. (5) in the Method's section. Different from [25–29], the agent uses a co-moving egocentric map, which allows to study motility noise. The expected change in information is the sum of two terms of information gain for SC and TC, respectively, and a loss term due to motility noise, see Eq. (6). Active motion with velocity $\mathbf{v}$ changes this expected information gain (to second order in the duration of the time-step), comprising an SC-term (equal to the spatial gradient of a rate of information gain from SC), and a TC-term (equal to a weighted gradient of the local rate of molecule detection), see Eq. (7). This analytical

theory, developed in [34], was rewritten here in more compact form to highlight information gain from SC and TC. While the originally nonlinear theory was numerically challenging, a simple linearization proposed here significantly speeds up simulations.

Without loss of generality, we assume that agents move with constant speed $v = |\mathbf{v}|$. Changing v can be compensated by rescaling time, which rescales λ and D_{rot}; likewise, changing concentration c is equivalent to changing λ.

The agent need to choose its direction of motion in each time step. We tested two prototypical decision rules, which maximize either exploitation or exploration of information, respectively. In a maximum-likelihood (ML) strategy maximizing exploitation, the agent moves straight towards the global maximum of the current likelihood map $p(\mathbf{x}, t)$. Infotaxis provides a second possible navigation strategy, in which the agent chooses its velocity vector $\mathbf{v}$ such that the expected change in information is maximized [25]. For our spatially extended agent, this is the case if $\mathbf{v}$ maximizes Eq. (7), which represents two possibly conflicting decision incentives, represented by a SC-term and the TC-term, respectively (see above). In the following, we study both strategies for different noise regimes and agent sizes.

1.3 Stereotypic navigation in absence of motility noise

We first simulated chemotactic agents without motility noise using either the maximum-likelihood strategy or infotaxis, see Fig. 2a. Agents using infotaxis display stereotypic behavior and first move along a straight path whose direction is determined by initial conditions. After a characteristic turning event that defines a time t_{turn}, these agents home in to the target along approximately circular arcs. In contrast, agents using a maximum-likelihood strategy display more erratic motion before they move approximately ballistically to the target. Snapshots of likelihood maps shown as insets indicate that agents can swiftly estimate target distance, but less so target direction, as reflected by the initially annulus-shaped likelihood map. As agents accumulate

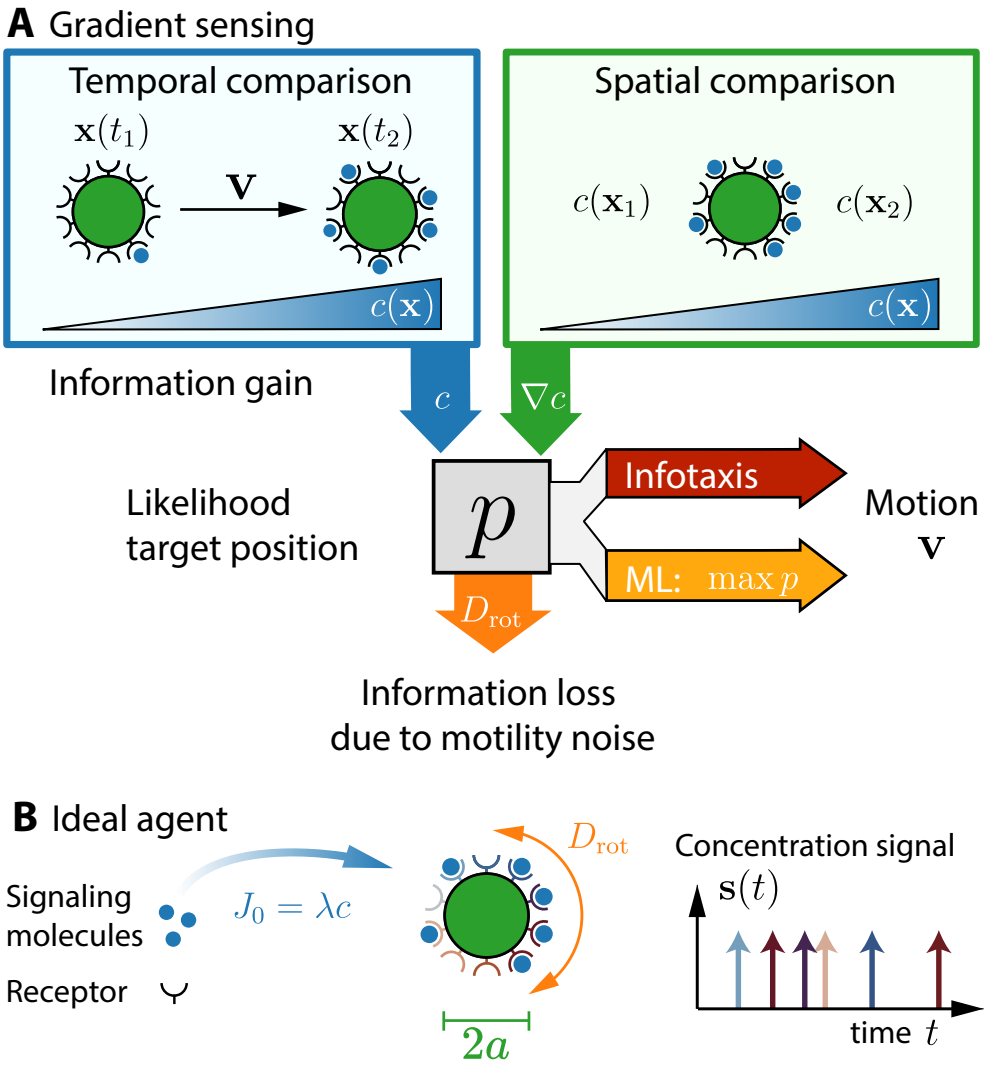

Fig. 1 Chemotactic navigation by temporal and spatial comparison. a Schematic of gradient-sensing by temporal comparison (TC), where chemotactic agents detect concentration differences along their motion path at different times (left), and spatial comparison (SC), where agents detect concentration differences across their diameter (right). These strategies represent information sources, from which agents can infer a likelihood map $p(\mathbf{x})$ of target position $\mathbf{x}$. Agents take decisions on their next motion step with velocity $\mathbf{v}$ based on this map using either maximum-likelihood (ML) or infotaxis. Motility noise randomizes motion direction and results in a continuous loss of information. **b** Model of an ideal agent that registers both time and position of signaling molecules binding at rate λc to receptors on its surface. The agent has size a; motility noise is modeled by an effective rotational diffusion coefficient D_{rot}.

directional information, these annulus-shaped distributions become crescent-shaped. Occasionally, distributions become bimodal when agents move towards the center of the crescent (where likelihood is high), but do not sense the expected increase in molecule detection frequency, thus erasing likelihood there, which splits the crescent in two.

We characterize the directional information of chemotactic agents by the Shannon information $I_\varphi = \int d\varphi\, p(\varphi)\, \log_2 p(\varphi)$ in bits of the marginal distribution $p(\varphi)$ of the polar angle φ of relative target direction. The ensemble average of this directional information increases monotonically in time at a characteristic rate of information gain set by the signal-to-noise ratio $\mathrm{SNR}^{\mathrm{TC}}$ of temporal comparison, Eq. (2), see Fig. 2b.

The characteristic turning events observed for infotaxis agents consistently occur when I_φ reaches the critical value of 1 bit, see Fig. 2c (Fig. S1 for more examples). This is exactly the amount of directional information needed to judge whether the target lies in one half-space or the other.

1.4 Information flow balance with motility noise

Motility noise, modeled as effective rotational diffusion with diffusion coefficient D_{rot}, sets a finite persistence length $l_p = v/D_{\mathrm{rot}}$ of agents, see Fig. 3, where $l_p = 1$ in Fig. 3a and $l_p = 0.2$ in Fig. 3b. The randomization of swimming direction causes a continuous loss of information on putative target position. The result is a quasi-steady state of information flow, where information gain due to chemo-sensation and information loss due to motility noise balance each other, reflected by a saturation of directional information $I_\varphi(t)$ at a maximal value I^*_φ, see Fig. 3c, d.

The mean angular information I^*_φ at this quasi-steady state collapses onto a master-curve $I^*_\varphi(X)$ with $X = \lambda^{0.28} D_{\mathrm{rot}}^{-0.68} a^{0.10}$ that combines the rate constant λ of molecule detection, D_{rot}, and agent size a into an effective power-law, see Fig. 3e, f. Power-law exponents were determined by linear regression of the logarithm of I^*_φ (for infotaxis)

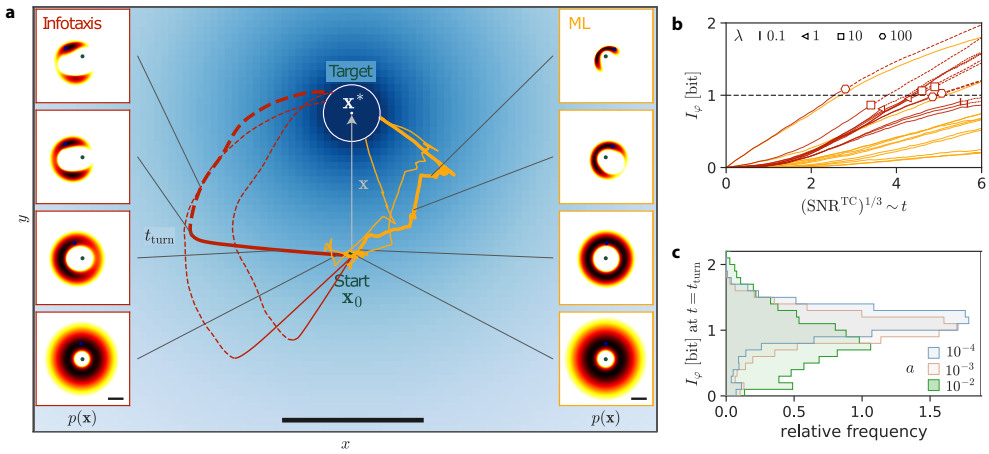

Fig. 2 Stereotypic motion without motility noise. a Typical trajectories of chemotactic agents (start point: green) navigating in a two-dimensional concentration field $c(x, y)$ of signaling molecules (blue) released by a target (dark-blue). Agents use either a maximum-likelihood decision rule (ML, orange), or infotaxis maximizing the expected information gain (red). Insets depict likelihood maps $p(\mathbf{x})$ at selected times for one example trajectory each. For infotaxis, we distinguish a first straight section of the trajectories (solid), and a second section (dashed) after a turning point at time $t_{\rm turn}$. Scale bar: 0.2 length units. **b** Angular information I_φ on target direction as function of renormalized time expressed in terms of a signal-to-noise ratio $\mathrm{SNR}^{\mathrm{TC}}$ of temporal comparison, Eq. (2), for infotaxis (red) and ML (orange), for different values of the rate constant λ of molecule detection and agent size a (ensemble mean; symbols for infotaxis indicate turning point with symbol shape indicating λ according to lengend and symbol size increasing with a). **c** Distribution of $I_\varphi(t_{\rm turn})$ at the first turning point for the case of infotaxis for different agent sizes (represented by line style, see legend; data pooled for different values of λ). Parameters: $D_{\rm rot} = 0$, a: $a = 10^{-4}$, $\lambda = 1$, b, c: $a = 10^{-4} - 10^{-2}$, $\lambda = 1 - 100$.

as function of the logarithms of the independent variables, which provides a robust collapse on a master-curve even for this nonlinear functional relationship. The behavior for the maximum-likelihood strategy is remarkably similar. The exponents of the power-law reflect the competition between information gain due to TC (characterized by λ) and SC (characterized by λa), and information loss (characterized by $D_{\rm rot}$). A similar power-law holds for the probability of agents to eventually find the target, see Fig. S2 in SM.

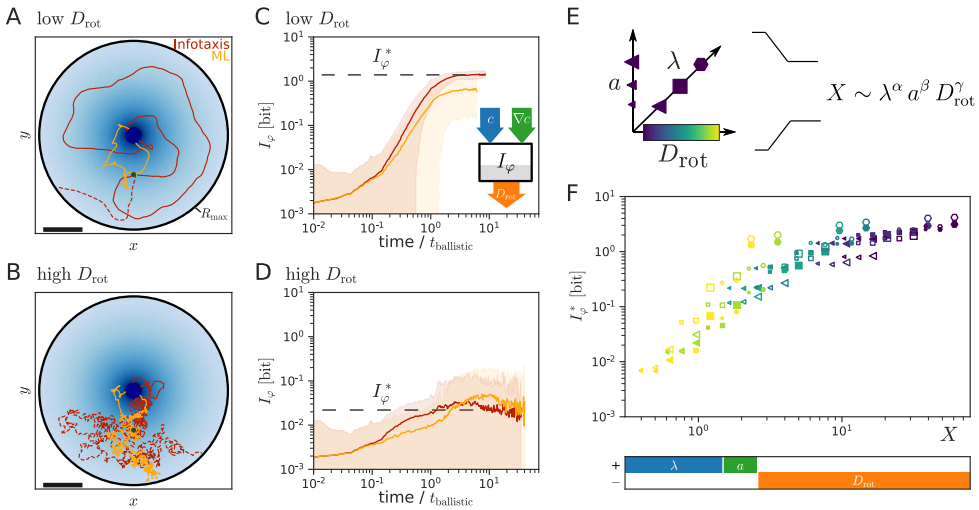

Fig. 3 Quasi-steady state of information flow with motility noise. a, b Typical trajectories of agents subject to motility noise using either a maximum-likelihood strategy (orange) or infotaxis (red) with low $D_{\rm rot}$ (panel **a**, $l_p = 1$) or high $D_{\rm rot}$ (panel **b**, $l_p = 0.2$). Dashed trajectories failed to find the target, but reached the absorbing boundary (black) at $R_{\max}$ before. Scale bar: 0.2 length units. **c, d** Directional information I_φ as function of normalized time $t/t_{\rm ballistic}$ with $t_{\rm ballistic} = R_{\rm target}/v$ for cases of low motility noise (panel **c**) and high motility noise (panel **d**) reveal a quasi-steady state of directional information with saturating directional information I_φ^* (orange: maximum-likelihood strategy, red: infotaxis; ensemble mean±s.d.). The inset in panel **c** sketches information flow determining I_φ, with information gained by TC (blue) and SC (green) and lost due to motility noise (orange). **e** The three fundamental model parameters (λ, $D_{\rm rot}$, a) can be combined into a single empirical power-law $X = \lambda^\alpha D_{\rm rot}^\beta a^\gamma$ for any simulated quantity such as I_φ^* to test if that quantity collapses on a master-curve as function of this single effective parameter X (with exponents determined by a linear fit of logarithms). **f** Quasi-steady states of directional information collapse on an empirical power law $I_\varphi^* = I_\varphi^*(X)$ with $X = \lambda^{0.28} D_{\rm rot}^{-0.62} a^{0.10}$. (maximum-likelihood strategy: open symbols, infotaxis: filled symbols; agent parameters encoded according to coordinate system in panel **e**). Power-law exponents are determined for infotaxis and visualized below the figure. Parameters (unless stated otherwise): a, c: $a = 0.01$, $\lambda = 1$, $D_{\rm rot} = 0.01$; b, d: same as a but $D_{\rm rot} = 0.5$; e, f: $a = 10^{-4} - 10^{-2}$, $\lambda = 1 - 100$, $D_{\rm rot} = 5 \cdot 10^{-3} - 1$.

1.5 Relative importance of spatial comparison

To gain further insight into the relative importance of temporal comparison (TC) versus spatial comparison (SC) for target finding, we computed their respective contributions to the directional information I_φ. While information decomposition remains challenging in general, we can make use of our analytical theory. For each information source, we computed the corresponding information gains $dI_\varphi^{\rm TC}$ and $dI_\varphi^{\rm SC}$ to I_φ using partial updates that involve only that term on the right-hand side of the update

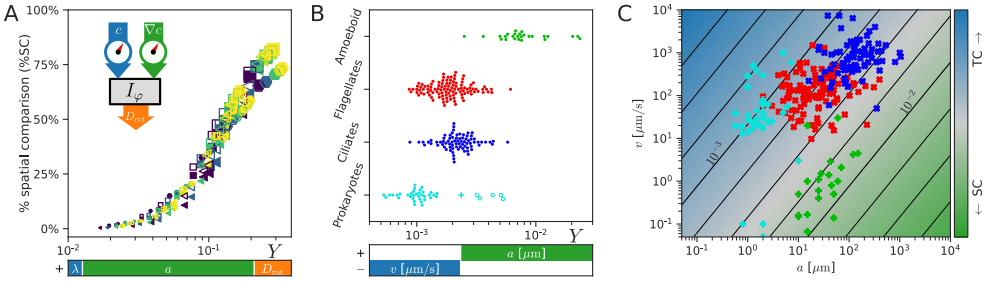

Fig. 4 Information decomposition reveals relative importance of spatial comparison. **a** The relative importance of spatial comparison %SC for target finding, computed by metering information flow, collapses on an empirical power law %SC(Y) with $Y = \lambda^{0.06}\, D_{\rm rot}^{0.17}\, a^{0.77}$ (maximum-likelihood strategy: open symbols, infotaxis: filled symbols; agent parameters encoded according to inset in Fig. 3). Specifically, we computed the cumulated gain in directional information using partial update steps corresponding to temporal and spatial comparison according to Eq. (5), respectively, see text for details. Power-law exponents determined for infotaxis by linear fit. **b** Data of biological cells performing chemotaxis taken from [2] plotted according to the power-law from panel **a** making the conservative assumption that rotational diffusion is set by thermal fluctuations. The color code represents different navigation strategies: cyan: bacteria which perform gradient-sensing by temporal comparison (symbols, see text), blue and red: ciliates and flagellates performing helical klinotaxis representing a mixed strategy, green: eukaryotic cells with amoeboid motility performing chemotaxis by spatial comparison. The power-law can be equivalently expressed as $a^{0.31}/v^{0.23}$ in terms of directly measurable parameters size a and speed v, using an assumption on the diffusion coefficient (see SM). **c** Data from [2] replotted in a-v parameter space, together with the empirical power-law for the relative importance of spatial comparison as in panel **a** plotted as color code. Parameters: $a = 10^{-3} - 2\cdot 10^{-2}$, $\lambda = 1 - 100$, $D_{\rm rot} = 0.1 - 1$, B: $c = 1\,$nM.

equation Eq. (5) that corresponds to this information source. By integrating over trajectories and averaging, we thus obtain the mean cumulated information gains, $I_\varphi^{\rm TC}$ and $I_\varphi^{\rm SC}$, for TC and SC, respectively (conditioned on agents that found the target), see SM text for details. Fig. 4a shows the relative fraction $\%{\rm SC} = I_\varphi^{\rm SC} \,/\, (I_\varphi^{\rm TC} + I_\varphi^{\rm SC})$ of the information gain for SC as function $\%{\rm SC}(Y)$ of a second empirical power law $Y = \lambda^{0.06}\, D_{\rm rot}^{0.17}\, a^{0.77}$ obtained by a linear fit. As expected, agent size a is the presiding factor determining the relative importance of spatial comparison. Motility noise ($D_{\rm rot}$) increases the contribution of spatial comparison, while sensing noise ($\sim 1/\lambda$) slightly decreases its contribution, as reflected by the positivity of the respective exponents. This dependence on motility noise is consistent with the notion that reduced directional persistence negative impacts TC.

While our theoretical analysis considers an ideal agent with unlimited information processing capabilities, it is not directly clear whether the behavior of biological cells

is dictated by similar laws. Therefore, we re-analyzed data from 252 different cell types corresponding to four groups (prokaryotes, ciliates, flagellates, cells with amoeboid motility) as reviewed in [2]. Fig. 4b shows for each cell type the value of the power-law derived in Fig. 4a for the ideal agent. Prokaryotes are known to perform gradient-sensing by TC. Ciliates and flagellates employ a mixed strategy known as helical klinotaxis combining aspects of TC and SC reviewed below. Cells with amoeboid motility use chemotaxis by SC [5–7]. Fig. 4b demonstrates that these cells employ temporal or spatial comparison exactly when our theory of ideal agents indicates a higher relative importance of one versus the other. For this comparison, agent sizes and speeds as reported in [2] were converted to values of the parameters λ, D_{rot}, a, using a conservative estimate for D_{rot} that assumes rotational diffusion is set by thermal fluctuations, hence $D_{\mathrm{rot}} \sim a^{-3}$, while the diffusive flux of signaling molecules to the agent scales linearly with its size, $\lambda \sim a$ [15]. With these assumptions, and a rescaling of time to account for different speeds of cells, we can re-map parameters and re-state the empirical power-law from Fig. 4a in terms of the directly measurable parameters cell size a (measured in μm), and speed v (measured in μm/s), see Fig. 4b bottom and the equivalent representation in Fig. 4c. Explicitly, we used the initial target distance R_{target} as typical length-scale and $t_{\mathrm{ballistic}} = R_{\mathrm{target}}/v$ as typical time-scale, to write the power-law from Fig. 4a first in dimensionless form, and then, using the scaling of D_{rot} and λ, in terms of the directly measurable quantities size a and speed v

$$\%\mathrm{SC}(Y) : Y \sim (\lambda c\, t_{\mathrm{ballistic}})^{0.06}\, (D_{\mathrm{rot}}\, t_{\mathrm{ballistic}})^{0.17}\, (a/R_{\mathrm{target}})^{0.77} \sim \frac{a\,[\mu\mathrm{m}]^{0.32}}{v\,[\mu\mathrm{m/s}]^{0.23}}\,, \quad (3)$$

see SM for details.

By Eq. (3), additional factors can affect the relative importance of SC. A bacterium described in [41] displays chemotaxis by SC at very high oxygen concentrations, corresponding to a 5000-fold increase of λc relative to the reference value used here.

This unusual bacterium is marked by a cross in Fig. 4b. Other bacteria that seem to deviate from the rule (open circles in Fig. 4b), either perform phototaxis instead of chemotaxis, or display unusual types of motility, such as pili-based motility or actin polymerization [2].

Ciliates and flagellates shown in Fig. 4b, c employ a navigation strategy known as helical klinotaxis [2, 14, 42]. As in TC with a single effective sensor, these cells sample a scalar signal along their swimming path. Yet, swimming paths are helical, so in the course of a single helical turn, this sensor will have probed all directions, just as agents performing SC, thus enabling directed steering. Eq. (1) could be extended to helical klinotaxis if instead of a the radius R of helical swimming paths is used. Helical klinotaxis is most efficient in three space dimensions, and only possible if the persistence time D_{rot}^{-1} exceeds the period $T \sim R/v$ of helical swimming [2, 3].

In conclusion, our information-theoretic analysis explains the previous heuristic observation that large and slow cells commonly employ spatial comparison for gradient-sensing, while small and comparatively fast cells use temporal comparison instead [1, 2, 43].

1.6 A phototactic robot

As proof-of-principle that bio-inspired Bayesian chemotaxis combining TC and SC may be applied in autonomous search robots (instead of using only TC [44–46]), we built a phototactic robot equipped with an circular array of light sensors, see Fig. 5a. As proxy for a scalar field corrupted by shot noise, this robot navigates in response to a fluctuating pixel pattern projected on the floor, using Bayesian inference as used in simulations. Camera-based tracking yields robot tracks that strongly resemble those in simulations, see Fig. 5b. Changing the size of the sensory array provides a simple means to probe different effective sensing length-scales a. The relative importance of spatial comparison in the corresponding robot experiments (computed analogously to

Fig. 4b) agrees well with simulation results, despite actuator noise, demonstrating the feasibility of the approach, see Fig. 5c.

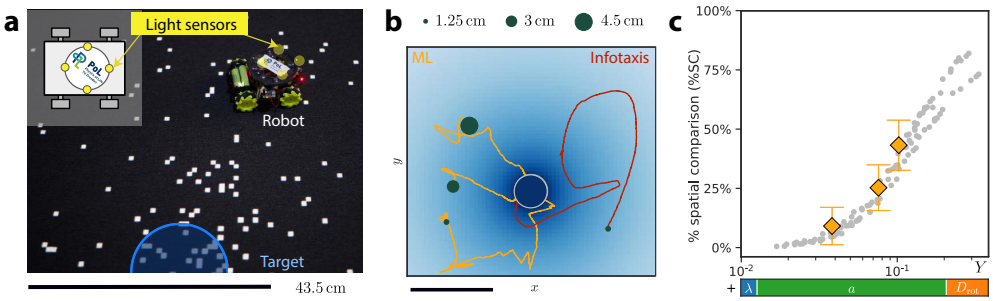

Fig. 5 A phototactic robot combining spatial and temporal comparison. a Search robot equipped with array of 4 light sensors exposed to a fluctuating pixel pattern projected on the floor. Robots navigate in response to this light stimulus using the same algorithm as ideal agents to find the center of a radial gradient of stochastically flashing pixels. **b** Typical tracks of robots using either maximum-likelihood decision strategy (ML, orange) or infotaxis (red) with different sensor array sizes (green dots mark start positions; tracks rotated for visual clarity). **c** The relative importance of spatial comparison (%SC) for target finding in experiments with ML-robots with different sensor array sizes (red, mean±s.d., $n = 22, 10, 14$) matches simulation data for simulated agents from Fig. 4a (gray dots), using a measured estimate $D_{\mathrm{rot}} = 0.004$, see SM for details. Scale bars in a, b: 43.5 cm (which maps to 0.2 length units).

2 Discussion

We used information theory to compare two fundamental gradient-sensing strategies for chemotaxis, *spatial comparison* (SC) and *temporal comparison* (TC), by quantifying their relative importance in an agent that combines both. Specifically, a minimal model of an ideal agent with unlimited information processing capabilities allowed us quantify 'chemotaxis in bits' in a baseline scenario. An analytical theory allows explicit information decomposition and thus to dissect the relative importance of SC versus TC, which collapses on a master-curve. The corresponding power-law reflects the expected competition between size a and speed v [1, 2, 43], additionally tuned by the level of motility noise. The relative importance of SC increases with increasing motility noise, as reduced directional persistence negatively impacts TC.

The ideal chemotactic agent introduced here unifies previous work of either point-like chemotactic agents [20, 21, 25, 26] (only TC), or extended, but mostly stationary agents [16, 17, 38, 47] (only SC). An early computational work that addressed the importance of SC versus TC in a one-dimensional model (neglecting motility noise and assuming specific signaling circuits), identified the ratio between cell size and speed already as key discriminator for the relative importance of SC [43], inline with the heuristic rule used in [2] and in agreement with our more general result.

Our analysis thus provides a theoretical foundation for the previous heuristic notion on the evolutionary choice of different chemotaxis strategies in different cell types [1–3], which could be summarized as small and fast cells use TC, while large and slow (and less persistent) cells use SC. The power-law derived here for a minimal model provides a robust predictor for this choice of chemotaxis strategy in single-celled organisms, see Fig. 4.

We tested two prototypical decision rules, which represent two extremes of the fundamental exploitation-exploration trade-off: *maximum-likelihood* (ML) and *infotaxis*. Both strategies exhibit similar performance, underscoring the generality of our results. While ML confines agents to the proximity of the target, resulting in a slight overall advantage, infotaxis initially performs better, as the persistent motion of agents right after their start increases information gain from TC. Thus, a mixed strategy, which balances exploitation and exploration, may optimize performance.

Bayesian chemotaxis requires agents to have a model of typical search environments, yet should be robust with respect to deviations between internal model and reality [38, 48]. Supplemental simulations show that chemotactic agents still exhibit similar performance even if the assumed sensing-noise parameter or rotational diffusion coefficient used in their update step differ from the true values used to generate the input signal and simulate their motion (Figs. S6 and S7). In biological cells, such knowledge about the environment (including characteristic dynamic changes of

the environment [8, 21, 28, 29, 32, 37]) is likely hard-wired in biochemical signaling networks and learned through evolutionary adaptation.

Although single-celled organisms likely do not possess the information processing capabilities to perform Bayesian chemotaxis, the run-and-tumble motion of the bacterium *E. coli* shares features with the behavior of infotaxis agents in the limit of low motility noise, which comprises a straight run followed by a turn, which would be repeated if there were an information reset after each turn. Biased random walks as observed for amoeboid cells in shallow gradients [6], emerge naturally in our minimal model. We thus expect that information-theoretically optimal chemotaxis as studied here for an ideal agent, which weights gradient-sensing in space and time, can shed light on the evolutionary choice of different gradient-sensing strategies under the pressure of sensing and motility noise.

3 Methods

3.1 Analytical theory

We review a minimal model of an ideal chemotactic agent subject to tunable sensing and motility noise previously developed in our group [34], and adapted for efficient simulations here. We first recall the mathematical theory from [34]. Eqs. (5-7) below are directly based on results derived there, though rewritten in more compact form that highlights information gain from SC and TC.

Following [34], we consider a disk-shaped agent of radius a and center position $\mathbf{x}_0(t)$, which searches for a hidden target at unknown position $\mathbf{x}^* = \mathbf{x}_0 + \mathbf{x}$ in the plane. The agent can detect signaling molecules diffusing from the target at each point $\mathbf{x_e} = \mathbf{x}_0 + a\mathbf{e}$ of its circumference at a rate density $\lambda c(\mathbf{x_e})/(2\pi a)$ proportional to the local concentration $c(\mathbf{x_e})$, where $c(\mathbf{x}) \sim 1/|\mathbf{x}|$ denotes the steady-state profile established by

diffusion from a spherical source. We introduce a vector-valued *chemotactic signal* [38]

$$\mathbf{s}(t) = \sum_j \mathbf{e}_j \, \delta(t - t_j) \quad , \tag{4}$$

which records binding events occurring at time t_j at position $\mathbf{x}_0 + a\,\mathbf{e}_j$ on the agent's circumference, modeled as an inhomogeneous Poisson process, see Supplemental Material (SM) for details, and Fig. 1b for visualization. The absolute value $s(t) = |\mathbf{s}(t)| = \sum \delta(t - t_j)$ is simply the train of binding events, ignoring their point of detection, as considered in [25]. If the target is assumed to be located at relative position $\mathbf{x}$, the conditional expectation value $\mathbb{E}(\mathbf{s}\,|\,\mathbf{x}) = \lambda a \nabla c/2$ of the vector signal $\mathbf{s}(t)$ encodes the local concentration gradient, while $J = \mathbb{E}(s\,|\,\mathbf{x})$ equals the rate of molecular binding events. This rate is proportional to the mean concentration along the circumference of the agent, $J \approx \lambda[c(\mathbf{x}_0) + (a^2/4)\nabla^2 c(\mathbf{x}_0)]$ [34].

The agent moves inside the concentration field with constant speed $v = |\mathbf{v}|$, subject to rotational diffusion with effective rotational diffusion coefficient D_{rot}, providing a minimal model of motility noise [38]. This dynamics extends the popular model of an Active Brownian Particle (ABP) [49], as our agent shall continuously decide on its direction of motion based on the directional chemo-sensory input it receives.

We are interested in the information-theoretic limits of chemotaxis, and therefore assume unlimited information processing capabilities of the agent, which can store and update a likelihood map $p(\mathbf{x}, t)$ of relative target position $\mathbf{x} = \mathbf{x}^* - \mathbf{x}_0$. The choice of an *egocentric map*, in which the moving agent is always at the center (with coordinate axes aligned to a co-moving material frame of the agent), is mathematically convenient. We assume that the agent has implicit knowledge of stereotypic concentration fields, and hence knows the conditional rate $J(\mathbf{x}_0|\mathbf{x}^*)$ and concentration gradient $\nabla_{\mathbf{x}_0} c(\mathbf{x}_0|\mathbf{x}^*)$, provided the target were at $\mathbf{x}^* = \mathbf{x}_0 + \mathbf{x}$. Here, ∇c points towards the target.

Bayes' rule rationalizes how to update previous beliefs in light of new information. In a time-continuous formulation, the time-evolution of a likelihood map $p(\mathbf{x},t)$ of relative target position reads

$$\frac{\partial}{\partial t}p(\mathbf{x},t) = \underbrace{\Big(\mathbf{s} - \mathbb{E}(\mathbf{s}|s>0)\Big)\cdot\left(\frac{a\nabla c}{c} - \frac{\langle a\nabla c\rangle}{\langle c\rangle}\right)\frac{Jp}{\langle J\rangle}}_{\text{SC}} + \underbrace{(s-\mathbb{E}\,s)\left(\frac{J}{\langle J\rangle}-1\right)p}_{\text{TC}} + \underbrace{D_{\text{rot}}\frac{\partial^2 p}{\partial\varphi^2}}_{\text{motility noise}} + \underbrace{\mathbf{v}\cdot\nabla p}_{\text{co-advection}} + \mathcal{O}(a^2)\,, \quad (5)$$

which follows from [34] after linearization by moment-closure, see SM for details. This approximation is key for efficient numerical simulations. The expectation values $\mathbb{E}\,s$ and $\mathbb{E}(\mathbf{s}|s>0)$ denote measurements expected by the agent given its current likelihood map $p(\mathbf{x},t)$, while $\langle\cdot\rangle$ averages over $\mathbf{x}$, again using $p(\mathbf{x},t)$. Thus, $\mathbb{E}\,s = \langle\mathbb{E}(s\,|\,\mathbf{x})\rangle$. Each summand on the right-hand side of Eq. (5) has a straight-forward physical interpretation. The third summand describes loss of information due to motility noise characterized as rotational diffusion, where φ denotes the polar angle of $\mathbf{x}$. The last summand describes the motion-induced shift of the egocentric map, in which the the relative position of the target changes as $\dot{\mathbf{x}} = -\mathbf{v}$ when the agent moves with velocity $\mathbf{v}$. The TC-term describes the update of target position based on the detection of signaling molecules, yet without reference to their position of detection on the circumference of the agent, thus generalizing TC. This term is equivalent to an analytical theory developed previously in [26] for the point-like agents introduced in [25], and has a simple geometric interpretation: whenever binding events are recorded at a rate higher than the expected detection rate (i.e., $s>\langle J\rangle$), the likelihood $p(\mathbf{x})$ is increased for all target positions $\mathbf{x}$, for which the local detection rate is higher than this mean rate ($J(\mathbf{x})>\langle J\rangle$), but decreased for all other positions. For $s<\langle J\rangle$, this update has the

opposite sign. In particular, even the absence of a binding event provides information to the agent, namely that the target might be further away than expected [50].

The SC-term is novel, and describes the update due to spatial comparison of concentration differences across the diameter of the agent. This term is a scalar product of an innovation vector, formed by the difference of the vector-valued concentration measurement $\mathbf{s}(t)$ and its conditional expectation value $\mathbb{E}(\mathbf{s}|s > 0) = \mathbb{E}\mathbf{s}\, s / \langle J \rangle$ if a binding event has happened, and the local concentration gradient, likewise corrected by a suitable expectation baseline. If no binding event is detected, the innovation vector is zero, reflecting the fact that it is impossible to record the position of a binding event without noticing that there has been a binding event in the first place.

Expected change in information. From the current prior $p(\mathbf{x}, t)$, the agent can infer the likelihood to detect a signaling molecule at a particular position, and thus forecast how the Shannon information $I = \int d\mathbf{x}\, p(\mathbf{x}) \ln p(\mathbf{x})$ is expected to change in the infinitesimal time interval $[t, t + dt]$ ahead, see [34] and SM text for details

$$\mathbb{E}\,\frac{d}{dt} I = \underbrace{\frac{1}{4}\left\langle J \left| \frac{a\nabla c}{c} - \frac{\langle a \nabla c \rangle}{\langle c \rangle} \right|^2 \right\rangle}_{\text{SC}} + \underbrace{\left\langle J \ln\left(\frac{J}{\langle J \rangle}\right)\right\rangle}_{\text{TC}} + \underbrace{D_{\text{rot}} \langle \frac{\partial^2}{\partial \varphi^2} \ln p \rangle}_{\text{motility noise}} + \mathcal{O}(a^3) \quad . \tag{6}$$

The SC-term characterizes information gain due to spatial comparison and is always non-negative. If multiplied by a characteristic sensing time, this term generalizes the signal-to-noise ratio SNR^{SC} of spatial comparison, see Eq. (1), by accounting for the expected gradient baseline $\langle \nabla c \rangle$. The TC-term characterizes information gain due to temporal comparison; it is always ≥ 0 because it is proportional to the Kullback-Leibler divergence between the likelihood maps p and $p\, J / \langle J \rangle$ before and after a

binding event, respectively. The last summand characterizes information loss due to motility noise; this Fisher information is always ≤ 0 by Bruijn's inequality [34].

Active motility with velocity $\mathbf{v}$ affects the expected change of information only to second order in the time-step, which can be expressed in terms of the time derivative of the expected change in information

$$\frac{d}{dt}\left(\mathbb{E}\,\frac{d}{dt}I\right) = C + \underbrace{\left\langle \nabla\left(\frac{J}{4}\left|\frac{a\nabla c}{c} - \frac{\langle a\nabla c\rangle}{\langle c\rangle}\right|^2\right)\right\rangle \cdot \mathbf{v}}_{\text{SC}} + \underbrace{\left\langle \ln\left(\frac{J}{\langle J\rangle}\right)\nabla J\right\rangle \cdot \mathbf{v}}_{\text{TC}} + \mathcal{O}(a^3) \quad , \quad (7)$$

where C combines terms independent of $\mathbf{v}$. Eq. (7) reformulates a result in [34] in more compact form, see SM for details. The first term characterizes information gain due to SC whereas the second term characterizes information gain due to concentration sensing akin to TC.

4 Data availability

Simulation data is available at https://zenodo.org/record/8421582 under DOI 10.5281/zenodo.8421582. Data analyzed in Fig. 4 on speed and size of chemotactic cells is available as Supplemental Data of [2].

5 Code availability

Python code for efficient simulation of Bayesian chemotaxis investigated here is available at https://zenodo.org/record/8421582 under same DOI 10.5281/zenodo.8421582.

6 Acknowledgments

JR, MN, BMF were supported by the German National Science Foundation (DFG) through FR3429/3-1 to BMF, the *Center for Advancing Electronics Dresden* (cfaed), and the Excellence Initiative by the German Federal and State Governments (Clusters of Excellence cfaed EXC-1056 and 'Physics of Life' (PoL) EXC-2068 - 390729961). BMF is additionally supported by the DFG through FR3429/4-1, 4-2 (Heisenberg grant). We thank Andrea Auconi for stimulating discussions. We thank Camillo Oeser and Arthur Willert for help with experiments.

7 Supplementary information

Supplementary Materials

Supplementary Figs. S1-S9, including extended numerical and analytical methods.

Supplementary videos

Supplementary videos show the time evolution of the likelihood map $p(x, y, t)$ of target position in the laboratory frame of reference for simulated agents and robot experiments (agent: green disk drawn to scale, or green cross if too small; target: blue). Panels to the right show the directional information $I_\varphi(t)$ as function of time t, where the red line indicates current time, as well as a cartoon representation of the agent visualizing molecular binding events relative to the material frame of the agent. The coordinate system inside the agent depicts the laboratory frame of reference.

Supplementary video 1

Agent without motility noise performing infotaxis.

Supplementary video 2

Agent without motility noise using maximum-likelihood strategy.

Supplementary video 3

Agent with motility noise performing infotaxis.

Supplementary video 4

Agent with motility noise using maximum-likelihood strategy.

Supplementary video 5

Robot experiment for maximum-likelihood strategy.

References

[1] Dusenbery, D. B. Spatial sensing of stimulus gradients can be superior to temporal sensing for free-swimming bacteria. *Biophys. J.* **74**, 2272–2277 (1998).

[2] Wan, K. Y. & Jékely, G. Origins of eukaryotic excitability. *Phil. Trans. R. Soc. B* **376**, 20190758 (2021).

[3] Alvarez, L., Friedrich, B. M., Gompper, G. & Kaupp, U. B. The computational sperm cell. *Trends Cell Biol.* **24**, 198–207 (2014).

[4] Zigmond, S. H. Mechanisms of sensing chemical gradients by polymorphonuclear leukocytes. *Nature* **249**, 450–452 (1974).

[5] Parent, C. A. & Devreotes, P. N. A cell's sense of direction. *Science* **284**, 765–770 (1999).

[6] Van Haastert, P. J. & Postma, M. Biased random walk by stochastic fluctuations of chemoattractant-receptor interactions at the lower limit of detection. *Biophys. J.* **93**, 1787–1796 (2007).

[7] Amselem, G., Theves, M., Bae, A., Beta, C. & Bodenschatz, E. Control parameter description of eukaryotic chemotaxis. *Phys. Rev. Lett.* **109**, 1–5 (2012).

[8] Nakajima, A., Ishihara, S., Imoto, D. & Sawai, S. Rectified directional sensing in long-range cell migration. *Nat. Commun.* **5**, 5367 (2014).

[9] Berg, H. C. & Brown, D. A. Chemotaxis in *Escherichia coli* analysed by three-dimensional tracking. *Nature* **239**, 500–504 (1972).

[10] Macnab, R. M. & Koshland, D. E. The gradient-sensing mechanism in bacterial chemotaxis. *Proc. Natl. Acad. Sci. U.S.A.* **69**, 2509–2512 (1972).

[11] Segall, J. E., Block, S. M. & Berg, H. C. Temporal comparisons in bacterial chemotaxis. *Proc. Nat. Acad. Sci. U.S.A.* **83**, 8987–8991 (1986).

[12] Brumley, D. R. *et al.* Bacteria push the limits of chemotactic precision to navigate dynamic chemical gradients. *Proc. Natl. Acad. Sci. U.S.A.* **166**, 10792–10797 (2019).

[13] Mattingly, H. H., Kamino, K., Machta, B. B. & Emonet, T. *Escherichia coli* chemotaxis is information limited. *Nat. Phys.* **17**, 1426–1431 (2021).

[14] Jikeli, J. F. *et al.* Sperm navigation along helical paths in 3D chemoattractant landscapes. *Nat. Commun.* **6**, 7985 (2015).

[15] Berg, H. C. & Purcell, E. M. Physics of chemoreception. *Biophys. J.* **20**, 193 (1977).

[16] Endres, R. G. & Wingreen, N. S. Accuracy of direct gradient sensing by single cells. *Proc. Natl. Acad. Sci. U. S. A* **105**, 15749–15754 (2008).

[17] Hu, B., Chen, W., Rappel, W.-J. & Levine, H. Physical limits on cellular sensing of spatial gradients. *Phys. Rev. Lett.* **105**, 048104 (2010).

[18] Bialek, W. & Setayeshgar, S. Physical limits to biochemical signaling. *Proc. Natl. Acad. Sci. U.S.A.* **102**, 10040–10045 (2005).

[19] Kaizu, K. *et al.* The Berg-Purcell limit revisited. *Biophys. J.* **106**, 976–985 (2014).

[20] Mora, T. & Wingreen, N. S. Limits of sensing temporal concentration changes by single cells. *Phys. Rev. Lett.* **104**, 248101 (2010).

[21] Hein, A. M., Brumley, D. R., Carrara, F., Stocker, R. & Levin, S. A. Physical limits on bacterial navigation in dynamic environments. *J. R. Soc. Interface* **13** (2016).

[22] Fuller, D. *et al.* External and internal constraints on eukaryotic chemotaxis. *Proc. Natl. Acad. Sci. U.S.A.* **107**, 9656–9659 (2010).

[23] Thornton, K. L., Butler, J. K., Davis, S. J., Baxter, B. K. & Wilson, L. G. Haloarchaea swim slowly for optimal chemotactic efficiency in low nutrient environments. *Nat. Commun.* **11**, 4453 (2020).

[24] Nakamura, K. & Kobayashi, T. J. Optimal sensing and control of run-and-tumble chemotaxis. *Phys. Rev. Res.* **4**, 013120 (2022).

[25] Vergassola, M., Villermaux, E. & Shraiman, B. 'Infotaxis' as a strategy for searching without gradients. *Nature* **445**, 406 (2007).

[26] Barbieri, C., Cocco, S. & Monasson, R. On the trajectories and performance of infotaxis, an information-based greedy search algorithm. *EPL* **94**, 20005 (2011).

[27] Loisy, A. & Eloy, C. Searching for a source without gradients: how good is infotaxis and how to beat it. *Proc. R. Soc. A* **478**, 20220118 (2022).

[28] Rigolli, N., Magnoli, N., Rosasco, L. & Seminara, A. Learning to predict target location with turbulent odor plumes. *eLife* **11**, e72196 (2022).

[29] Reddy, G., Murthy, V. N. & Vergassola, M. Olfactory sensing and navigation in turbulent environments. *Annu. Rev. Condens. Matter Phys.* **13**, 191–213 (2022).

[30] Celani, A. & Vergassola, M. Bacterial strategies for chemotaxis response. *Proc. Natl. Acad. Sci. U.S.A.* **107**, 1391–1396 (2010).

[31] Hartl, B., Hübl, M., Kahl, G. & Zöttl, A. Microswimmers learning chemotaxis with genetic algorithms. *Proc. Natl. Acad. Sci. U.S.A* **118**, e2019683118 (2021).

[32] Stocker, R. Marine microbes see a sea of gradients. *Science* **338**, 628–633 (2012).

[33] Lange, S. & Friedrich, B. M. Sperm chemotaxis in marine species is optimal at physiological flow rates according theory of filament surfing. *PLoS Comput. Biol.* **17**, e1008826 (2021).

[34] Auconi, A., Novak, M. & Friedrich, B. M. Gradient sensing in Bayesian chemotaxis. *EPL* **138**, 12001 (2022).

[35] Kobayashi, T. J. Implementation of dynamic bayesian decision making by intracellular kinetics. *Phys. Rev. Lett.* **104**, 1–4 (2010).

[36] Kromer, J., Märcker, S., Lange, S., Baier, C. & Friedrich, B. M. Decision making improves sperm chemotaxis in the presence of noise. *PLoS Comp. Biol.* **14**, 1–15 (2018).

[37] Mora, T. & Nemenman, I. Physical limit to concentration sensing in a changing environment. *Phys. Rev. Lett.* **123**, 198101 (2019).

[38] Novak, M. & Friedrich, B. M. Bayesian gradient sensing in the presence of rotational diffusion. *New J. Phys.* **23**, 043026 (2021).

[39] Bain, A. & Crisan, D. *Fundamentals of stochastic filtering* (Springer, 2009).

[40] Strong, S. P., Freedman, B., Bialek, W. & Koberle, R. Adaptation and optimal chemotactic strategy for *E. coli*. *Phys. Rev. E* **57**, 4604–4617 (1998).

[41] Thar, R. & Kühl, M. Bacteria are not too small for spatial sensing of chemical gradients: An experimental evidence. *Proc. Natl. Acad. Sci. U.S.A.* **100**, 5748–5753 (2003).

[42] Crenshaw, H. A new look at locomotion in microorganisms: rotating and translating. *Am. Zool.* **36**, 608–618 (1996).

[43] Tan, R. Z. & Chiam, K.-H. A computational model for how cells choose temporal or spatial sensing during chemotaxis. *PLoS Comput. Biol.* **14**, e1005966 (2018).

[44] Moraud. Effectiveness and robustness of robot infotaxis for searching in dilute conditions. *Front. Neurorobot.* (2010).

[45] Masson, J.-B. Olfactory searches with limited space perception. *Proc. Natl. Acad. Sci. U.S.A* **110**, 11261–11266 (2013).

[46] Voges, N., Chaffiol, A., Lucas, P. & Martinez, D. Reactive searching and infotaxis in odor source localization. *PLoS Comput. Biol.* **10**, e1003861 (2014).

[47] Dobramysl, U. & Holcman, D. Triangulation sensing to determine the gradient source from diffusing particles to small cell receptors. *Phys. Rev. Lett.* **125**, 148102 (2020).

[48] Rodríguez, J. D., Gómez-Ullate, D. & Mejía-Monasterio, C. On the performance of blind-infotaxis under inaccurate modeling of the environment. *Euro. Phys. J. Spec. Topics* **226**, 2407–2420 (2017).

[49] Romanczuk, P., Bär, M., Ebeling, W., Lindner, B. & Schimansky-Geier, L. Active Brownian particles. *Eur. Phys. J. Spec. Top.* **202**, 1–162 (2012).

[50] Hein, A. M. & McKinley, S. A. Sensing and decision-making in random search. *Proc. Natl. Acad. Sci. U.S.A.* **109**, 12070–12074 (2012).

Symbol	Description
a	agent size
$\mathbf{x}_0$	agent position
$\mathbf{x}^*$	target position
$\mathbf{x}$	relative target position $\mathbf{x} = \mathbf{x}^* - \mathbf{x}_0$
$\mathbf{v}$	velocity vector of agent
v	speed of agent
D_{rot}	rotational diffusion coefficient of agent
$c(\mathbf{x}_0\|\mathbf{x}^*)$	concentration field of signaling molecules, provided target at $\mathbf{x}^*$
λ	rate constant of molecule detection, $J_0(\mathbf{x}) = \lambda c(\mathbf{x})$
$\mathbf{s}(t)$	vector-valued concentration signal, see Eq. (4)
$s(t)$	$= \|\mathbf{s}\|$ train of molecular binding events
$J_0(\mathbf{x})$	$= \lambda c(\mathbf{x})$ rate of molecule detection for a single receptor
$J(\mathbf{x})$	$= \mathbb{E}(s \,\|\, \mathbf{x})$ rate of molecule detection, provided target at $\mathbf{x}^* = \mathbf{x}_0 + \mathbf{x}$
	$\approx \lambda[c(\mathbf{x}_0) + (a^2/4)\nabla^2 c(\mathbf{x}_0)]$
$\mathrm{SNR}^{\mathrm{SC}}$	$= a^2 t\lambda\|\nabla c\|^2/c$ signal-to-noise ratio for spatial comparison, Eq. (1),
$\mathrm{SNR}^{\mathrm{TC}}$	$= v^2 t^3 \lambda\|\nabla c\|^2/c$ signal-to-noise ratio for temporal comparison, Eq. (2),
R_0	initial target distance
R_{target}	target size
R_{max}	radius of simulation domain (with absorbing boundary conditions)
t_{turn}	time till first turn for case $D_{\mathrm{rot}} = 0$
$t_{\mathrm{ballistic}}$	characteristic time for ballistic motion
P_{reached}	probability to reach target
I_φ	directional information [in bits]
I_φ^*	quasi-steady state of directional information, see Fig. 3
$I_\varphi^{\mathrm{TC+SC}}$	cumulated directional information: contribution due to TC and SC
$I_\varphi^{D_{\mathrm{rot}}}$	cumulated directional information: contribution due to motility noise
I_φ^{adv}	cumulated directional information: contribution due to advection
I_φ^{TC}	cumulated directional information: contribution due to TC
I_φ^{SC}	cumulated directional information: contribution due to SC
$\mathbb{E}(s)$	$= \langle J\rangle/2 \approx \lambda[\langle c\rangle + (a^2/4)\langle\nabla^2 c\rangle]$ expectation value of molecular binding events $s(t)$
$\mathbb{E}(\mathbf{s})$	$= \lambda a\langle\nabla c\rangle/2$ expectation value of the vector signal $\mathbf{s}(t)$
$\mathbb{E}(\mathbf{s}\|s>0)$	$= \mathbb{E}\mathbf{s}\, s/\langle J\rangle = s\lambda a\langle\nabla c\rangle/(2\langle J\rangle)$ conditional expectation value of vector signal $\mathbf{s}(t)$

Table 1 List of symbols.